Pergamon

Acta Materialia 50 (2002) 4357–4367

Acta MATERIALIA

www.actamat-journals.com

Anomalous thermal stability of Nd–Fe–Co–Al bulk metallic glass

B.C. Wei [a,*], W. Löser [b], L. Xia [c], S. Roth [b], M.X. Pan [c], W.H. Wang [c], J. Eckert [b]

[a] *National Microgravity Laboratory, Institute of Mechanics, Chinese Academy of Sciences, Beijing 100080, People's Republic of China*

[b] *IFW Dresden, Institute for Metallic Materials, PO Box 270016, D-01171 Dresden, Germany*

[c] *Institute of Physics and Center for Condensed Matter Physics, Chinese Academy of Sciences, Beijing 100080, People's Republic of China*

Received 2 April 2002; received in revised form 24 June 2002; accepted 1 July 2002

Abstract

The thermal stability of $Nd_{60}Fe_{20}Co_{10}Al_{10}$ bulk metallic glass (BMG) has been studied by differential scanning calorimetry (DSC), dynamic mechanical thermal analysis (DMTA), isochronal dilatation and compression tests. The results show that the glass transition of the BMG takes place quite gradually between about 460 and 650 K at a heating rate of 0.17 K/s. Several transformation processes are observed during continuous heating with the first crystallization process beginning at about 460 K, while massive crystallization takes place near the solidus temperature of the alloy. The positive heat of mixing between the two major constituents, Nd and Fe, and, consequently, a highly inhomogeneous composition of the attained amorphous phase are responsible for the anomalous thermal stability in this system.

Keywords: Casting; Rare earth alloys; Metallic glass; Heterogeneous phase transformations

1. Introduction

Intensive efforts have been carried out over the past decade to develop alloy systems with critical cooling rates below 100 K/s for glass formation, i.e., with good glass-forming ability (GFA). The estimation of the GFA in metallic alloy systems is of special importance as it can provide guidelines for the production of metallic glasses, especially in bulk form. Various empirical criteria have been proposed to reflect the GFA of alloys in previous studies [1–5]. Turnbull proposed that the reduced glass transition temperature T_{rg}, defined as the glass transition temperature T_g divided by the liquidus temperature T_l, could be regarded as a measure to evaluate the GFA of an alloy [1]. This correlation has been confirmed in many experiments [6]. Inoue and Masumoto adopted the temperature difference ΔT_x between T_g and the first crystallization

* Corresponding author. Tel.: +86-10-82649198; fax: +86-10-62615524.

E-mail address: weibc@imech.ac.cn (B.C. Wei).

1359-6454/02/$22.00
PII: S1359-6454(02)00272-0

event (T_x) upon heating at a constant rate as a measure for the stability of the supercooled liquid above T_g [4]. It has been demonstrated that larger values of ΔT_x tend to be correlated with lower values of the critical cooling rate R_c necessary for glass formation for some bulk metallic glass-forming (BMG) systems, such as Ln–Al–TM, Mg–Ln–TM, Zr–Al–TM, Ti–Zr–TM and Zr–Ti–TM–Be (Ln: lanthanide metal, TM: transition metal) systems [7,8].

More recently, Nd–TM–Al BMGs have been prepared by slow cooling from the melt [9–19]. Depending on the thermal stability, such alloys can be subdivided into two categories: one class of alloys are iron-free or iron-poor systems, for example $Nd_{60}Co_{30}Al_{10}$, $Nd_{60}Ni_{10}Cu_{10}Co_5Al_{15}$ and $Nd_{60}Fe_5Co_{10}Cu_{10}Al_{15}$ etc., showing a normal thermal stability with T_{rg} near 0.6 and ΔT_x around 40 K [9,11,12]. The other type of alloys is iron-rich systems, for example, $Nd_{60}Fe_{30}Al_{10}$, $Nd_{60}Fe_{20}Co_{10}Al_{10}$, and $Nd_{57}Fe_{20}Co_5Al_{10}B_8$ etc. The latter systems do not exhibit a distinct glass transition prior to crystallization starting at T_x according to constant-rate heating DSC measurements, indicating a low thermal stability of the supercooled liquid [10–19]. However, an extremely high value of the ratio between the T_x and T_l around 0.9 was observed for such systems, which indicates a rather high stability of the amorphous phase against crystallization [10,11,14,15,18,19]. The contradiction between the absence of a distinct glass transition and the extremely high value of T_x/T_l shows that these systems are rather unique within the different families of BMGs.

To clarify the thermal stability of the Fe-rich Nd-based alloys is important for the following reasons. First, one can verify the validity of the existing empirical criteria for evaluating the GFA of such alloys, otherwise a new and more widely applicable criterion is needed. The second is that it will be helpful to understand the good GFA for this system, since rods with diameters up to 15 mm have been produced by suction casting [10,11]. Furthermore, this system together with the similar Pr–Fe–Al system are the only two systems exhibiting hard magnetic properties in as-cast "amorphous state" up to now [10–20]. A better understanding of the thermal stability of these systems will also contribute to a better evaluation of possible applications for these magnetic materials.

In this work, the thermal stability of $Nd_{60}Fe_{20}Co_{10}Al_{10}$ BMG was studied systematically by means of differential scanning calorimetry (DSC), dynamic mechanical thermal analysis (DMTA), dilatometric measurements, and compression tests. Based on the results obtained by the different techniques, the reasons for the anomalous thermal stability of Fe-rich BMGs and the reason for the difference between Fe-rich and Fe-poor systems will be discussed.

2. Experimental

Pre-alloyed $Nd_{60}Fe_{20}Co_{10}Al_{10}$ ingots were prepared by arc-melting a mixture of Nd, Fe, Co, and Al elements with a purity of at least 99.9% in titanium-gettered argon atmosphere. Cylindrical specimens of 3 mm in diameter and 70 mm in length were prepared from the pre-alloyed ingots by suction casting into a copper mold. Ribbons were obtained by melt-spinning with a single copper wheel under pure argon atmosphere. The structure of the cast cylinders and the melt-spun ribbons was characterized by X-ray diffraction (XRD) in a Philips PW 1050 diffractometer using Co Kα radiation. Thermal analysis was performed with a Perkin-Elmer DSC 7 differential scanning calorimeter under argon atmosphere. A constant heating rate of 0.17 K/s was employed. The Curie temperature (T_c) was measured by thermomagnetic analysis (TMA) using a Faraday magnetometer at a heating rate of 0.17 K/s. The dynamic mechanical properties were measured at a heating rate of 0.17 K/s by using a dynamic mechanical thermal analyzer (Rheometric Scientific DMTA IV) in three-point bending mode. The samples for these measurements were cut from the middle part of the cylinders and had a size of $1.2 \times 3.0 \times 30$ mm^3. The applied static load was 1 N and the frequency for the dynamic load was 1 Hz. The thermal expansion was measured on cylinder samples, 3 mm in diameter, under a compressive load of 0.3 N. The experiments were performed using a NETZSCH DIL 402C dilatometer with a resolution of $\Delta L =$ 1.25 nm. A low heating rate of 0.017 K/s was used

to ensure the temperature homogeneity in the sample during heating. The compression tests on cylindrical samples of 3 mm in diameter and 5.8 mm in length were performed in an Instron-type testing machine at various temperatures from room temperature up to 723 K. The specimens were equilibrated for about 300 s at each test temperature before testing. The cross-head was moved at a constant speed with an initial strain rate of 5.0×10^{-3} s^{-1}. The microstructure of the samples after compression testing was studied by a Cambridge scanning electron microscope (SEM) equipped with a Link energy dispersive X-ray (EDX) microanalysis system in back scattering mode. A Digital Instruments NanoScope IIIa D-3000 atomic force microscope (AFM) was used to reveal the topographic features of the as-quenched ribbons.

3. Results

3.1. DSC results

The as-cast cylinders exhibit an XRD pattern typical for an amorphous phase without obvious crystalline reflections. Fig. 1 compares the DSC curve of the as-cast $Nd_{60}Fe_{20}Co_{10}Al_{10}$ BMG with the scan of a thin ribbon produced at a wheel speed of 18 m/s. No obvious endothermic heat flow event due to a glass transition is observed in the DSC traces. The pronounced exothermic peak with an onset temperature (T_x) of around 750 K corresponds to massive crystallization of the amorphous phase. These phenomena agree well with previously published results on Nd-based amorphous alloys [10–19]. A detailed study on the DSC traces (see inset in Fig. 1) shows that there are already exothermic processes in the lower temperature range for both the BMG and the ribbon. The heat flow signal deviates from the base line at temperatures as low as about 460 K, and a more obvious exothermic signal is observed above 580 K with a peak temperature of about 690 K for the BMG sample. For the ribbon, a low temperature exothermic peak with an onset temperature of 460 K appears, followed by two other exothermic peaks at 580 and 670 K, respectively. The magnitude of these exothermic processes in the temperature range from 460 to about 700 K are much weaker than the exothermic events corresponding to the massive crystallization at 770 K in both the BMG and the ribbon. All the exothermic reactions are irreversible processes, as each of them disappears for annealed samples in a second heating run.

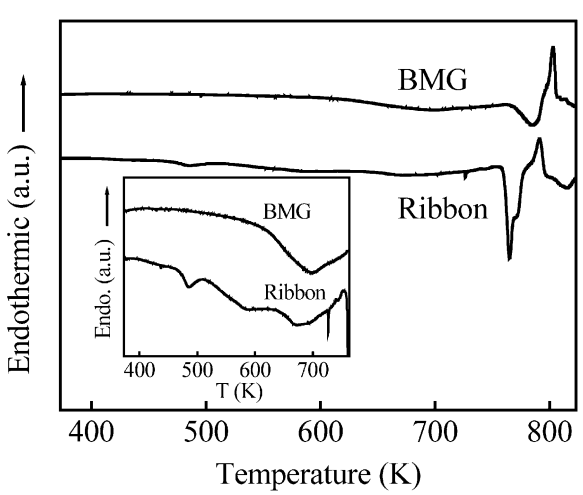

Fig. 1. DSC curves of the as-cast $Nd_{60}Fe_{20}Co_{10}Al_{10}$ BMG and a ribbon melt-spun at 18 m/s. The inset shows the enlarged part of the DSC scan revealing the exothermic peaks in the low temperature region.

3.2. Dynamic mechanical analysis and compression tests

The DSC results for $Nd_{60}Fe_{20}Co_{10}Al_{10}$ BMG are more complicated than those of the other BMG systems, for which a clear endothermic effect due to a glass transition is followed by one or several exothermic peaks caused by crystallization. In order to clarify the thermal stability of the present BMG, different types of tests were carried out. DMTA results for the as-cast bulk sample and for samples annealed at 603 and 708 K, respectively, are shown in Fig. 2a. Starting from room temperature, the storage modulus (E') of the as-cast sample decreases slightly as expected for conventional metals. The specimen softens markedly at about 498 K, and E' decreases rapidly from 48 MPa at 498 K to 31 MPa at 588 K. Subsequently, E' shows a weak peak with an onset temperature of 588 K, and then decreases continuously with further

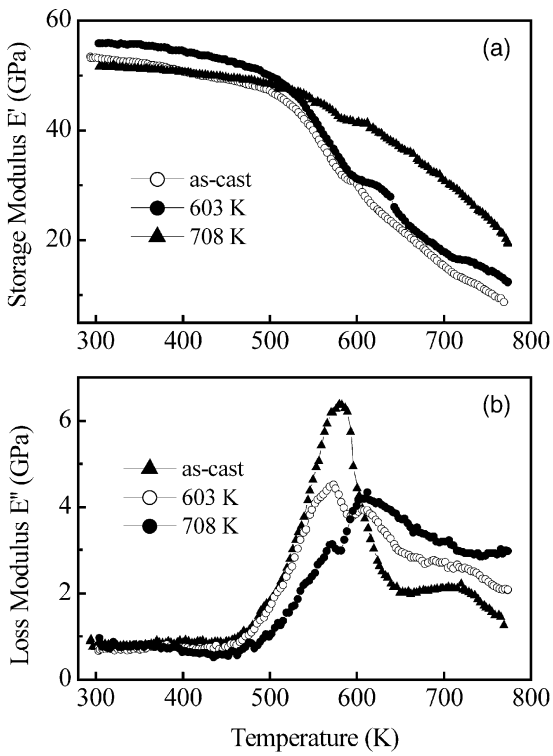

Fig. 2. DMTA results for as-cast and annealed $Nd_{60}Fe_{20}Co_{10}Al_{10}$ BMG: dependence of storage modulus (E') vs. temperature (a), and loss modulus (E'') on temperature (b).

increasing temperature. The most obvious feature for the loss modulus (E'') curve of the as-cast specimen (Fig. 2b) is the two connected sharp peaks of E'' ranging from 460 to 650 K, with peak temperatures of 571 and 581 K, respectively. In the higher temperature region, a weak and broad E'' peak occurs around 700 K, which corresponds to the broad exothermic peak in the same temperature range in the DSC curve (Fig. 1). During the DMTA measurement, a sinusoidal stress is applied. E' is the value of the energy which is stored and recovered perfectly during one cycle of stress change, while E'' is the loss of energy which changes into heat during one cycle, and corresponds to the internal friction, thus representing the degree of heat loss during one cycle. When $E' >> E''$, then E' is approximately equal to the complex modulus ($E^* = E' + iE''$), i.e. Young's modulus.

Internal friction is known to be sensitive to structural changes, and has been used to study the structural relaxation, the glass transition and the crystallization behavior of amorphous alloys [21–25]. The structural relaxation and crystallization generally lead to an increase of the modulus. However, in the present case, the marked E'' peak is accompanied by the rapid decrease of E'. Hence, it is suggested that the E'' peak in the DMTA curve is caused mainly by a glass transition process. Strong evidence supports this opinion, since this E'' peak is also observed for the samples annealed at the temperature higher than 600 K as shown in Fig. 2b, confirming that the internal friction peak is a reversible phenomenon (strictly speaking it is a partial reversible phenomenon).

In order to further confirm the existence of a glass transition process in the $Nd_{60}Fe_{20}Co_{10}Al_{10}$ BMG, additional compression tests were carried out. The temperature dependence of the stress–strain curves at an initial strain rate of 5.0×10^{-3} s^{-1} is shown in Fig. 3 (the nonlinear feature at the very beginning of each curve is an instrumental artifact in the early stage of the measurements). The samples were equilibrated for about 300 s at each test temperature before testing. The alloy is extremely brittle at room temperature with a fracture stress of about 510 MPa and no plastic deformation. The deformation mode changes from inhomogeneous deformation to homogeneous deformation at around 523 K, and the samples exhibit a marked plastic deformation at tempera-

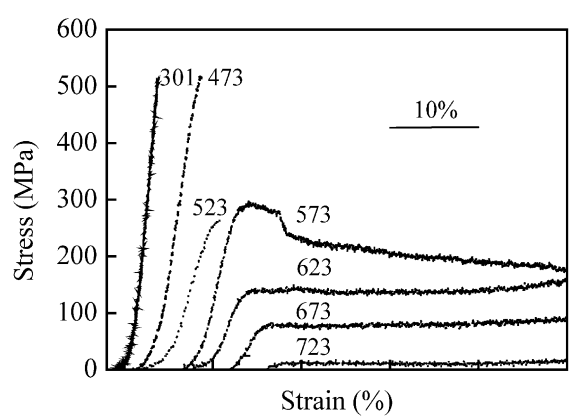

Fig. 3. Stress–strain curves as a function of testing temperature at an initial strain rate of 5.0×10^{-3} s^{-1}.

tures above 573 K. This further supports the assumption of the presence of a glass transition process as already suggested from the DMTA results. In addition, a stress overshoot followed by a viscous flow approaching a steady state can be seen in the curve measured at 573 K. For higher temperatures, this stress overshoot phenomenon disappears again. Such a stress overshoot phenomenon and a very similar temperature dependence of the deformation behavior were also observed for Zr-, Pd-, Mg-, and La-based metallic glasses at temperatures near T_g [26–31].

3.3. Thermal expansion measurements

The thermal expansion is also sensitive to the structural change of amorphous alloys. Extensive studies of the thermal expansion of amorphous alloys show that dilatation measurements, when combined with other characterization measurements, are helpful for understanding structural relaxation and crystallization of metallic glasses [32–35]. Fig. 4a shows the length change of the $Nd_{60}Fe_{20}Co_{10}Al_{10}$ as-cast BMG sample, ΔL, during repeated heating and cooling cycles of the same sample at a heating and cooling rate of 0.017 K/s. Only the heating processes are shown in the figure to avoid confusion. In the first run (heating from room temperature to 573 K), a decrease of the slope (representing the thermal expansion coefficient, α) around 410 K is observed during the continuous heating of the sample. In the second run (heating from room temperature to 673 K), a decrease of the slope occurs at 410, 570 and 630 K, respectively. As the sample was heated up to 573 K in the first run, the repeated appearance of the decrease of the slope around 410 K in the second run indicates that there is a reversible component for the decrease of the slope above 410 K in the first run. The decrease of the slope above 570 K corresponds to the exothermic reaction in DSC curve at about the same temperature even when considering the higher heating rate used for the DSC scans (see inset in Fig. 1). In the third run (heating from room temperature to 783 K), the reversible decrease of the slope around 410 K appears again, but the decrease at 570 and 630 K does not take place. Instead, a gradual increase of

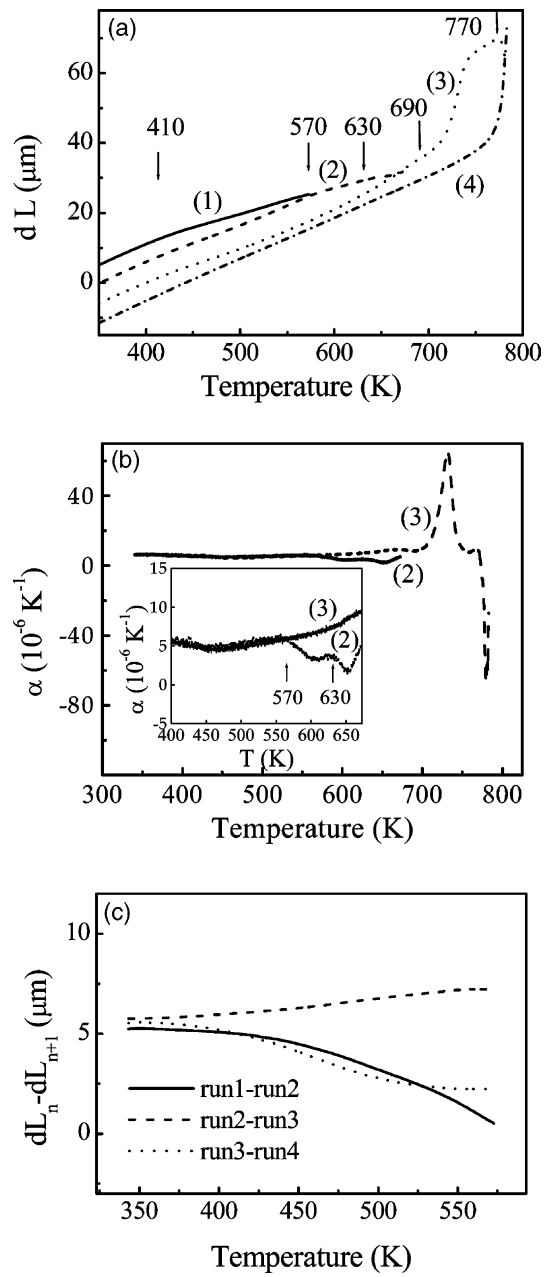

Fig. 4. (a) Temperature dependence of the length change of $Nd_{60}Fe_{20}Co_{10}Al_{10}$ BMG during repeated heating and cooling cycles (only the heating curves are shown) at a heating rate of 0.017 K/s and a compressive load of 0.3 N. The arrows point to the temperatures where the slopes change. (b) Linear expansion coefficient of the sample in the second and third runs. (c) Difference dilatation curves obtained from (a) in the following way: "curve 1−curve 2", "curve 2−curve 3", and "curve 3−curve 4".

the expansion coefficient is observed in the temperature range from 570 to 673 K. The temperature dependences of linear expansion coefficients α of the sample in the second and the third runs are plotted in Fig. 4b. The increase in α above 570 K in the third run is highlighted in the inset of Fig. 4b. At about 690 K, a decrease in α is revealed, which again corresponds to the temperature range of the exothermic peak in the DSC curve. A marked increase in α is observed from 713 to 743 K, followed by a rapid contraction of the sample at 770 K, corresponding to the sharp exothermic DSC peak due to the massive crystallization (Fig. 1). After cooling, a fourth heating run (heating from room temperature to 783 K) of the crystallized sample was performed, showing a nearly linear dependence of thermal expansion on temperature until about 773 K, where the sample expands strongly due to the melting of the crystalline phases.

As the $Nd_{60}Fe_{20}Co_{10}Al_{10}$ metallic glass is ferromagnetic at room temperature [14,17], one should consider the effect of ferromagnetic transitions on the length change of the sample. The TMA result of the as-cast BMG is shown in Fig. 5, and the result of a ribbon melt-spun at 18 m/s is also presented for comparison. The Curie temperature T_c of the as-cast BMG is determined to be 479 K, and a rapid decrease of magnetization with heating

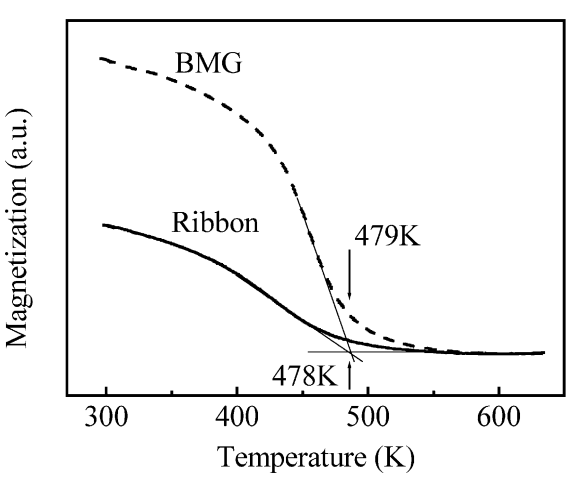

Fig. 5. Thermomagnetic analysis of the as-cast BMG and a ribbon melt-spun at 18 m/s.

is found in the temperature range from 410 to 479 K, which coincides with the temperature range where the reversible decrease of α takes place in the second and the third run of the dilatometer measurements. Previous results have proved that annealing at temperatures below 723 K has little effect on the room temperature magnetization of the Nd–Fe–Al based BMGs [10,11,13,17]. This means that the ferromagnetic transition of the BMG is a reversible process, and gives rise to the reversible decrease of α below T_c. The Curie transition of the BMG takes place in a temperature range much lower than that of the E'' peak in Fig. 2b. Hence, the internal friction peak of the BMG is not caused by a ferromagnetic transition.

Fig. 4c illustrates the difference of a dilatation run and the subsequent run, i.e. "run1−run2", "run2−run3", and "run3−run4". It can be seen that the decrease in α in the first run is not a fully reversible process, and a distinct irreversible component is found in the curve of "run1−run2", beginning at about 460 K. This corresponds to the slight deviation of the heat flow signal in the DSC curve around 460 K for the BMG (inset in Fig. 1), indicating that this is an exothermic process. In the DSC curve for the ribbon with the same composition, it is noted that an exothermic peak starts from about 460 K (inset in Fig. 1). This peak has been proved to be an early step of crystallization, as isothermal annealing at 453 K gives rise to a "bell-shape" exothermal peak, indicating that both nucleation and growth processes take place [36]. The BMG should possess a highly relaxed structure compared with the ribbon produced by melt-spinning because of the lower cooling rate during copper mold casting. Accordingly, quenched-in nuclei, clusters or nanocrystals may be present in the as-cast BMG [11], and the subtle exothermic effect and the irreversible decrease of α are probably due to the growth of the quenched-in nuclei or nanocrystals by consuming the amorphous phase. A weak reversible endothermic signal typical for a glass transition closely followed by a weak exothermic crystallization peak at around 450 K was also revealed by Li et al. for a $Nd_{60}Fe_{30}Al_{10}$ alloy using temperature modulated DSC at a heating rate of 0.017 K/s [12]. As the exothermic effect and the change in α in the

present case are very weak, it is assumed that only a small fraction of the amorphous phase crystallizes in this temperature range. The irreversible decrease in α at around 570 K in the second run of Fig. 4a is thought to be caused by the second stage of crystallization, as a small peak of E' and a sharp peak of E''' near this temperature are observed in the DMTA results (Fig. 2). Moreover, this temperature also corresponds to the onset temperature of the broad exothermic peak in the DSC curve (see inset in Fig. 1). The decrease in α at about 700 K in the dilatation measurements (the third run in Fig. 4a), corresponds to the broad exothermic peak in the DSC curve and the broad E'' peak. These results suggest that the third stage of crystallization takes place at around 700 K. The massive crystallization of the BMG is revealed by the sharp exothermic peak in the DSC curve at 770 K, and is confirmed by the dilatation measurement, which shows a rapid contraction of the sample. This significant crystallization process is not observed in the DMTA result because of the limitation of the measuring temperature range. Based on the above results, five crystallization processes at about 460, 570, 630, 700 and 770 K, respectively, occur in the BMG. The slight difference between run 2 and run 3 of the dilatation measurements ("run2−run3" in Fig. 4c) may be due to the higher amount of crystalline phases in run 3, while the irreversible component in "run2−run3" in Fig. 4c is caused by the loss of ferromagnetic properties for the crystallized alloy.

4. Discussion

4.1. The reason for the absence of T_g in DSC measurements

By combining dilatation measurements with DMTA, DSC and compression tests, one can reveal that, in the present $Nd_{60}Fe_{20}Co_{10}Al_{10}$ BMG a glass transition proceeds between about 460 and 650 K, and four weak crystallization processes take place at about 460, 570, 630 and 700 K, respectively, prior to the massive crystallization at 770 K. The superposition of the endothermic reaction due to glass transition and the exothermic reaction caused by the first crystallization process may be responsible for the absence of a clear T_g in the DSC measurements. However, in the DSC curve of the sample annealed at temperatures higher than T_g, the expected T_g due to the absence of the irreversible crystallization is still not observed. In the third run of the dilatation measurements (Fig. 4a and b), where the sample has already been heated up to 673 K, a gradual increase in the thermal expansion coefficient is observed above 570 K. This confirms that the majority of the alloy is already in a supercooled liquid state. The supercooled liquid can access additional configurational states of lower density, resulting in an increase in α [32–35]. These dilatation results further confirm the existence of a significant glass transition in the present BMG. However, no distinct inflection point in all the dilatation curves is observed which would clearly reveal the onset of the glass transition of the BMG.

To clarify the reason for the weak thermal and volume effect of glass transition in the present BMG, one has to consider the features of the Nd–Fe binary phase diagram [37]. Nd and Fe are the two main constituents in the $Nd_{60}Fe_{20}Co_{10}Al_{10}$ BMG, and possess a positive heat of mixing with each other. This is in contrast to other BMG forming systems, which exhibit large negative heats of mixing among the major constituents [11]. This means that upon cooling, Nd and Fe atoms tend to repulse each other, and few intermetallic compounds form in the equilibrium phase diagram [37]. The BMG alloy is close to the eutectic composition, and tends to form pure Nd on one hand and the stable Nd_2Fe_{17} phase on the other hand, if it is very slowly cooled [37]. Therefore, when copper mold cast, certain regions of the alloy tend to become enriched in Fe, and other regions tend to become Nd-rich. The overall composition of the alloy differs significantly from the compositions of the two eutectic phases. Hence a remarkable long-distance diffusion is needed for the precipitation of the equilibrium phases. Furthermore, the atoms in BMG alloys are densely packed, and the atomic diffusion coefficient is relatively low in these systems [11]. Consequently, the precipitation of the equilibrium phases is kinetically restricted and difficult in the present BMG, and the alloy tends to

solidify in a metastable state (e.g. amorphous state) beyond a critical cooling rate, rather than in the equilibrium state. This may be one of the reasons for the good GFA of the Nd–Fe–Al alloys. Similarly, Pr–Fe also exhibits a positive enthalpy of mixing [37]. Nd–Fe and Pr–Fe are the only two systems in the RE–Fe (RE=Ce to Lu) family, which possess a positive heat of mixing, while other systems exhibit a negative enthalpy of mixing and a larger number of intermetallic compounds [37]. Coincidentally, Nd–Fe–Al and Pr–Fe–Al have the largest glass-forming ability of RE–Fe–Al-based systems as far as it is known up to now. In other systems a $REFe_2$ Laves phase forms as a stable phase. This, in turn, significantly reduces the GFA [20,38,39].

Another consequence of the large compositional difference between the alloy and the eutectic phases is that the produced amorphous phase may possess a wide variety of local compositions, as the different parts of the sample undergo different local cooling conditions during casting. This means that the amorphous phase formed, in fact, comprises a series of amorphous states with different compositions, i.e. some areas are enriched in Fe, and other areas are enriched in Co or Al. Accordingly, the amorphous phase in the present BMG is probably a highly inhomogeneous system on a micro- or nanometer scale. The glass transition process in this system then occurs as revealed by the above results, but it takes place in a rather gradual manner because of the inhomogeneity of the composition of the amorphous phase. The compositional inhomogeneity is confirmed by the TMA results. The magnetization of the BMG decreases gradually below T_c, indicating the chemical inhomogeneity of the magnetic phase, while for the ribbon, where a larger difference of local cooling rate should be present in the sample, the gradual decrease of magnetization is more pronounced, as shown in Fig. 5. Furthermore, it is obvious from the DMTA results (Fig. 2b) that the E'' peak caused by the glass transition ends over a temperature range of about 190 K. The same measurement carried out for the well-known $Zr_{41}Ti_{14}Cu_{12.5}Ni_{10}Be_{22.5}$ alloy shows that the width of the E'' peak is about 90 K for this alloy [36]. The glass transition itself is a weak endothermic process, and it takes place gradually from 460 to 650 K in the present alloy system. This may be the major reason for the absence of a clear T_g in DSC measurements. The other reason concerns the Curie transition of the present ferromagnetic material, which is also a weak endothermic process, and also proceeds gradually from 410 to 479 K for the present alloy. The combination of these two weak endothermic events leads to the undistinguishable effect of both processes in the thermal analysis measurements.

4.2. The viscous flow and stress overshoot in $Nd_{60}Fe_{20}Co_{10}Al_{10}$ BMG

As shown in Fig. 3, a premature fracture is observed for the sample tested at room temperature, while at 473 K a slight plastic deformation occurs, which leads to the slight increase of the fracture stress. At the latter temperature, the early stage of the glass transition takes place, but is accompanied by the early stage of crystallization. Hence, at about 473 K the alloy is mainly composed of rigid amorphous solid plus a small amount of crystals, and, therefore, is still brittle. When the testing temperature is increased to about 523 K, the glass transition process proceeds, and the amount of the supercooled liquid increases. The plastic deformation occurs preferentially in the supercooled liquid region with lower viscosity, and giving rise to a distinct plastic strain. Upon further increasing the temperature, the stress overshoot is observed in the stress–strain curve at 573 K. The stress overshoot phenomenon has been studied in detail previously for $Zr_{65}Al_{10}Ni_{10}Cu_{15}$, $Zr_{55}Al_{10}Ni_5Cu_{30}$, $Zr_{52.5}Al_{10}Ti_5Cu_{17.9}Ni_{14.6}$, and $Pd_{40}Ni_{40}P_{20}$ metallic glasses [28–31]. Though the reasons for the presence of the stress overshoot in stress–strain curves are still a matter of debate in the literature, most authors tend to follow the reasoning that the stress overshoot is a result of a rapid increase in free volume during high strain rate deformation [28–31]. The stress overshoot in these BMG systems takes place generally at relatively high strain rates and at temperatures of around T_g. In contrast, the stress overshoot appears at the temperature far beyond T_g decided by the above analysis for the present BMG. The reason for this difference could

be that the glass transition takes place more gradually, and the early stage of the glass transition is followed by the weak crystallization process as stated above. Anyway, the appearance of the overshoot in the compressive stress–strain curve indirectly supports the presence of glass transition and supercooled liquid region in the present BMG.

On further increasing the test temperature the viscosity of the supercooled liquid decreases gradually, which causes the continuous decrease in the flow stress of the sample as shown in Fig. 3. A very localized viscous flow is observed in some areas of the back-scattering SEM image of the sample compressed at 673 K (not shown here). This indicates that the deformation behavior of the alloy is partially inhomogeneous at elevated temperatures.

4.3. Thermal stability of the amorphous phase and supercooled liquid phase in $Nd_{60}Fe_{20}Co_{10}Al_{10}$ BMG

As stated above, the composition of the amorphous phase in $Nd_{60}Fe_{20}Co_{10}Al_{10}$ BMG is inhomogeneous. Hence, the crystallization of the amorphous phase may also take place gradually. Certain parts of the amorphous phase with a local chemical and topological structure close to the crystalline counterparts, should crystallize prior to other parts, which are more different to the crystalline phases. Thus, different regions of the alloy crystallize in a sequence depending on the local structure, causing the appearance of the observed multi-stage crystallization, as revealed by the DSC and dilatation results. It is worth noting that the crystallization of the BMG spreads over a wide temperature range, and that massive crystallization only takes place near the solidus temperature T_s. In the temperature range between 620 and 770 K, the viscous flow behavior revealed by the stress–strain curve (Fig. 3), and the significant increase in thermal expansion coefficient α of the sample (Fig. 4a and b), demonstrate that the majority of the alloy is in the supercooled liquid state, even after the third crystallization stage at around 700 K. In other words, the remaining supercooled liquid is quite stable until massive crystallization sets in at about 770 K. The reason for this high thermal stability of the supercooled liquid in the BMG may be associated with a quite large compositional difference between the remaining supercooled liquid and the crystallization products. Hence, a remarkable long-range diffusion is needed for the nucleation and growth of the crystalline phases. This kinetic process requires a larger thermal activation, i.e. it occurs at a higher temperature than for most of the other BMGs, because of the larger chemical difference between the supercooled liquid and the equilibrium phases. An amorphous phase separation (APS) process then tends to occur to reduce the free energy of the system [40,41]. This APS takes place in the casting process due to the relatively slow cooling rate upon copper mold casting BMG, and leads to the inhomogeneity of the composition in the as-cast amorphous state. Fig. 6 displays an AFM image of the non-contact surface of a ribbon melt-spun at a low wheel speed (6 m/s). It can be seen that two continuous areas are observed with a width of each area of about 75 nm. This structural feature is similar to that in slowly cooled binary Nd–Fe ingots studied by SEM and TEM, in which two continuous areas are composed of pure Nd and Nd–Fe metastable phases, respectively [42]. The latter structure exhibits a larger scale due to the slower cooling rate and fewer atoms. Although the structure of the $Nd_{60}Fe_{20}Co_{10}Al_{10}$ ribbon produced at 6 m/s does not completely represent the structure of the BMG,

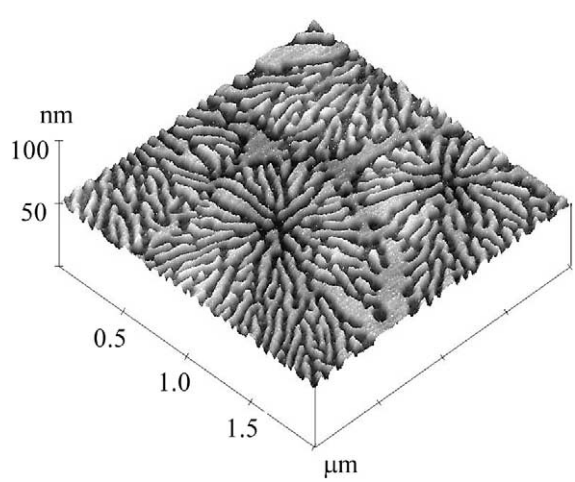

Fig. 6. Atomic force image of the ribbon melt-spun at 6 m/s.

it gives evidence that the alloy tends to form different nanoscale phases during cooling. Presumably, the structural feature in Fig. 6 results from a phase separation process in the melt or undercooled liquid state [43]. The APS process becomes more clear when the as-cast BMG is heated afterwards into the supercooled liquid region. As shown by the E'' curves (Fig. 2b), the single E'' peak for the as-cast BMG is split into two peaks for the samples annealed at 603 and 708 K, respectively. Both E'' peaks of the annealed samples are revealed to be reversible processes, as the annealing temperatures are higher than the two peak temperatures of E''. These results further suggest that a distinct APS occurs in the $Nd_{60}Fe_{20}Co_{10}Al_{10}$ BMG. Direct evidence of the APS is difficult to obtain, as this system may comprise a series of amorphous phases of different composition. The length-scale of the phase separation is roughly estimated to be tens of nanometers as indicated by Fig. 6.

5. Summary

Thermal analysis combined with dynamic mechanical analysis and dilatation measurements were used to characterize the thermal stability of $Nd_{60}Fe_{20}Co_{10}Al_{10}$ BMG. A glass transition process from about 460 to 650 K during continuous heating of the BMG is revealed by dynamic mechanical analysis, and further confirmed by dilatation results. The absence of the glass transition in DSC measurements and the multi-stage crystallization processes are attributed to the chemical inhomogeneity of the amorphous phase, and ultimately to the positive heat of mixing between Nd and Fe. A prominent thermal stability of the supercooled liquid is observed in this BMG, due to the large difference of composition between the amorphous phase and the competing crystalline phases. Furthermore, the tendency of a significant amorphous phase separation is also revealed for this alloy.

Acknowledgements

The authors are grateful to Z.R. Zhang, and B.S. Han for the AFM measurements, and to Z.G. Sun and G. Kumar for stimulating discussions. The financial support of the National Nature Science Foundation of China (Grant Nos. 50101012 and 50031010), and the Deutsche Forschungsgemeinschaft (DFG-Sonderforschungsbereich 463) is gratefully acknowledged.

References

[1] Turnbull D. Contemp. Phys. 1969;10:473.
[2] Uhlmann DR. J. Non-Cryst. Solids 1972;7:337.
[3] Davies HA, Lewis BG. Scripta mater. 1975;9:1109.
[4] Inoue A, Masumoto T. Mater. Sci. Eng. 1993;173A:1.
[5] Egami T. Mater. Sci. Eng. 1997;A226-A228:261.
[6] Lu ZP, Tan H, Li Y, Ng SC. Scripta mater. 2000;42:667.
[7] Inoue A, Zhang T, Masumoto T. J. Non-Cryst. Solids 1993;156-158:473.
[8] Shen TD, Schwarz RB. Appl. Phys. Lett. 1999;75:49.
[9] He Y, Price CE, Poon SJ, Shiflet GJ. Phil. Mag. Lett. 1994;70:371.
[10] Inoue A, Zhang T, Takeuchi A, Zhang W. Mater. Trans. JIM 1996;37:636.
[11] Inoue A, Takeuchi A, Zhang T. Metall. Mater. Trans. 1998;29A:1779.
[12] Li Y, Ng SC, Lu ZP, Feng YP, Lu K. Phil. Mag. Lett. 1998;78:213.
[13] Ding J, Li Y, Wang WZ. J. Phys. D: Appl. Phys. 1999;32:713.
[14] Xing LQ, Eckert J, Löser W, Roth S, Schultz L. J. Appl. Phys. 2000;88:3565.
[15] Fan GJ, Löser W, Roth S, Eckert J, Schultz L. Appl. Phys. Lett. 1999;75:2984.
[16] Wei BC, Zhang Y, Zhuang YX, Zhao DQ, Pan MX, Wang WH, Hu WR. J. Appl. Phys. 2001;89:3529.
[17] Wei BC, Wang WH, Pan MX, Han BS, Zhang ZR, Hu WR. Phys. Rev. B 2001;64:012406.
[18] Chiriac H, Lupu N. J. Non-Cryst. Solids 2001;287:135.
[19] Ortega-Hertogs RJ, Inoue A, Rao KV. Scripta mater. 2001;44:1333.
[20] Inoue A, Zhang T, Takeuchi A. Mater. Trans. JIM 1996;37:1731.
[21] Soifer YM, Kobelev NP, Brodova LG, Manukhin AN, Korin E, Soifer L. Nanostructured Mater. 1999;12:875.
[22] Chen HS, Morito N. J. Non-Cryst. Solids 1985;72:287.
[23] Waniuk TA, Busch R, Masuhr A, Johnson WL. Acta mater. 1998;46:5229.
[24] Rambousky R, Moske M, Samwer K. Mater. Sci. Forum 1995;179-181:761.
[25] Kimura H, Kishida M, Kaneko T, Inoue A, Masumoto T. Mater. Trans. JIM 1995;36:890.
[26] Inoue A, Nakamura T, Nishiyama N, Masumoto T. Mater. Trans. JIM 1992;33:937.
[27] Takagi M, Kawamura Y, Imura T, Nishigaki J, Saka H. J. Mater. Sci. 1992;27:817.

[28] Kawamura Y, Shibata T, Inoue A. Appl. Phys. Lett. 1997;71:779.
[29] Chen HS, Kato H, Inoue A. Mater. Trans. JIM 2001;42:597.
[30] Nieh TG, Wadsworth J, Liu CT, Ohkubo T, Hirotsu Y. Acta mater. 2001;49:2887.
[31] Reger-Leonhard A, Heilmaier M, Eckert J. Scripta mater. 2000;43:459.
[32] He Y, Schwarz RB, Mandrus DG. J. Mater. Res. 1996;11:1836.
[33] Lu I-R, Görler GP, Fecht H-J, Willnecker R. J. Non-Cryst. Solids 2000;274:294.
[34] Russew K. Mater. Sci. Eng. 1997;A226-228:779.
[35] Ludovit K. Key Eng. Mater. 1990;40-41:165.
[36] Wei BC, Wang WH, Zhang ZR, Han BS, Löser W, Roth S, Eckert J. Unpublished work.
[37] Massalski TB. Binary alloy phase diagrams, p. 1734. Materials Park, OH: ASM International, 1992.
[38] Fan GJ, Löser W, Roth S, Eckert J. Acta mater. 2000;48:3823.
[39] Kong HZ, Ding J, Wang L, Li Y. IEEE Trans. Magn. 2001;37:2500.
[40] Hays CC, Kim CP, Johnson WL. Appl. Phys. Lett. 1999;75:1089.
[41] Wang WH, Wei Q, Friedrich S. Phys. Rev. B 1998;57:8211.
[42] Delamare J, Lemarchand D, Vigier P. J. Alloys Compounds 1994;216:273.
[43] Schneider S, Bracchi A, Samwer K, Seibt M, Thiyagarajan P. Appl. Phys. Lett. 2002;80:1749.